

Control of the ZZ coupling between Kerr-cat qubits via transmon couplers

Takaaki Aoki,^{1,*} Taro Kanao,² Hayato Goto,² Shiro Kawabata,^{1,3} and Shumpei Masuda^{1,3,†}

¹*Research Center for Emerging Computing Technologies (RCECT),
National Institute of Advanced Industrial Science and Technology (AIST),
1-1-1 Umezono, Tsukuba, Ibaraki 305-8568, Japan*

²*Corporate Research and Development Center, Toshiba Corporation, 1,
Komukai-Toshiba-cho, Saiwai-ku, Kawasaki, Kanagawa 212-8582, Japan*

³*NEC-AIST Quantum Technology Cooperative Research Laboratory,
National Institute of Advanced Industrial Science and Technology (AIST),
1-1-1 Umezono, Tsukuba, Ibaraki 305-8568, Japan*

Kerr-cat qubits are a promising candidate for fault-tolerant quantum computers owing to the biased nature of their errors. The ZZ coupling between the qubits can be utilized for a two-qubit entangling gate, but the residual coupling causes unnecessary always-on gates and crosstalk. In order to resolve this problem, we propose a tunable ZZ -coupling scheme using two transmon couplers. By setting the detunings of the two couplers at opposite values, the residual ZZ couplings via the two couplers cancel each other out. We also apply our scheme to the $R_{zz}(\Theta)$ gate (ZZ rotation with angle Θ), one of the two-qubit entangling gates. We numerically show that the fidelity of the $R_{zz}(-\pi/2)$ gate is higher than 99.9% in a case of 16-ns gate time and without decoherence.

I. INTRODUCTION

Quantum computation [1] is expected to surpass classical computation in speed in specific problems such as prime factorization [2], database search [3], quantum chemistry [4], and machine learning [5]. A major obstacle is noise caused by the interaction between a computing system and its environment [6, 7]. In order to cancel out the noise and obtain reliable computational results, we must perform quantum error correction [8, 9]. This requires a considerable overhead cost, which makes difficult the construction of a large-scale fault-tolerant quantum computer [10, Sec. 3.2].

However, when the noise is biased, we can reduce the overhead [11]. As such [12–14], a Kerr-cat qubit, which uses two coherent states with opposite phases as logical states and whose bit-flip error is exponentially suppressed with its photon number [15, Sec. I] [16, Sec. S2], has attracted much attention in recent years [12–38]. Universal gate sets [17–19] and bias-preserving gates [12–14] for Kerr-cat qubits have been theoretically proposed. A full set of single-qubit gates on a Kerr-cat qubit has been performed experimentally [20]. Quantum annealing [21–30] and Boltzmann sampling [31] based on Kerr-cat qubits have also been studied theoretically.

A Kerr-cat qubit is realized by a Kerr parametric oscillator (KPO), which is an oscillator under parametric (squeezing) drive with Kerr nonlinearity larger than the single-photon loss rate (single-photon Kerr regime) [17, 19, 21, 25, 39]. A typical coupling between KPOs is the beam-splitter type [12, 13, 18, 19, 21–23, 25–28, 31, 33, 37, 38, 40]. This leads to the ZZ (longitudinal) coupling between Kerr-cat qubits [12, 18, 19, 21,

23, 25, 26, 31, 33, 37, 38], which can be utilized for an R_{zz} (ZZ -rotation) gate [12, 18, 19, 25, 37, 38], one of the two-qubit entangling gates. The serious practical problem is that the residual ZZ coupling when the R_{zz} gate is not performed causes crosstalk [41, 42], which prevents precise computing.

In other systems such as transmons, tunable couplers have been used to eliminate unwanted residual couplings [43–51], but not yet in KPO systems. In this paper, we propose a tunable ZZ -coupling scheme between two Kerr-cat qubits using two transmon couplers. In this scheme, the detuning of one of the couplers is modulated to control the amplitude of the effective ZZ coupling between the qubits. Importantly, the residual coupling can be eliminated when the detunings of the two couplers are set to opposite values.

Our scheme does not utilize resonance-frequency difference between KPOs unlike the cross-resonance gate [52–55], and thus can be implemented with identical KPOs. Therefore, it is expected that our scheme will reduce the complexity of design and fabrication of multi-KPO systems. Our scheme can also mitigate the frequency-crowding problem, which becomes significant especially when frequency differences between qubits are needed [42]. In addition, our scheme is compatible with KPO systems with lattice structures in contrast to the previous one which utilizes the phase difference between pump fields and can be applied only to simple KPO networks such as one dimensional chains [37, 40]. Therefore, our scheme is advantageous for system scale-up.

This article is organised as follows. In Sec. II, we introduce our system Hamiltonian and logical states of Kerr-cat qubits. In Sec. III, we explain how to switch on and off the ZZ coupling between the qubits. In Sec. IV, we numerically evaluate the residual coupling and the $R_{zz}(-\pi/2)$ -gate fidelity. Finally, we conclude this article in Sec. V.

* takaaki-aoki@aist.go.jp

† shumpei.masuda@aist.go.jp

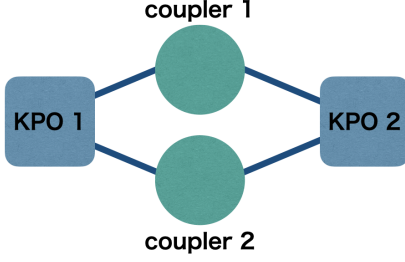


FIG. 1. Schematic diagram of the studied system. Two identical KPOs are coupled via two transmon couplers. Our arrangement is similar to that in Ref. [45, Fig. 1(a)].

II. SETTINGS

We consider a system consisting of two identical KPOs and two transmon couplers (see Fig. 1). The KPOs are parametrically driven with frequency ω_p which is twice their dressed resonance frequency ω^{KPO} [56, Appendix C]. The effective Hamiltonian of the system $\hat{H}(t)$ in a rotating frame at frequency $\omega_p/2$ is written, in rotating-wave approximation, as [38, Sec. II]

$$\hat{H}(t) = \sum_{j=1}^2 \hat{H}_j^{\text{KPO}} + \sum_{k=1}^2 \hat{H}_k^c(t) + \hat{H}_I, \quad (1)$$

$$\hat{H}_j^{\text{KPO}} = -\frac{K}{2} \hat{a}_j^{\dagger 2} \hat{a}_j^2 + \frac{p}{2} (\hat{a}_j^{\dagger 2} + \hat{a}_j^2), \quad (2)$$

$$\hat{H}_k^c(t) = -\frac{\chi_k}{2} \hat{c}_k^{\dagger 2} \hat{c}_k^2 + \Delta_k(t) \hat{c}_k^{\dagger} \hat{c}_k, \quad (3)$$

$$\hat{H}_I = \sum_{j,k=1}^2 g_{jk} (\hat{a}_j^{\dagger} \hat{c}_k + \hat{a}_j \hat{c}_k^{\dagger}), \quad (4)$$

where \hat{H}_j^{KPO} , $\hat{H}_k^c(t)$ and \hat{H}_I are the Hamiltonian of KPO j , the Hamiltonian of coupler k , and the interaction Hamiltonian, respectively; this interaction Hamiltonian corresponds to the capacitive couplings between the KPOs and the couplers [38, Appendix A]. Here, \hat{a}_j and \hat{c}_k are the annihilation operators of KPO j and coupler k ; $K(>0)$ and $p(>0)$ are the Kerr nonlinearity parameter and amplitude of the parametric drive of the KPOs; χ_k and $\Delta_k(t)$ are the Kerr nonlinearity parameter and detuning of coupler k ; $\Delta_1(t) := \omega_1^c(t) - \omega_p/2$ is time dependent but $\Delta_2 := \omega_2^c - \omega_p/2$ is not, where $\omega_1^c(t)$ (ω_2^c) is a tunable (fixed) resonance frequency of coupler 1 (2); g_{jk} is the coupling strength between KPO j and coupler k . We assume that $\chi_k = \chi(>0)$ and $g_{jk} = g(>0)$ throughout this paper for simplicity.

We can transform \hat{H}_j^{KPO} as

$$\hat{H}_j^{\text{KPO}} = -\frac{K}{2} (\hat{a}_j^{\dagger 2} - \alpha^2) (\hat{a}_j^2 - \alpha^2) + \frac{K\alpha^4}{2} \quad (5)$$

with $\alpha = \sqrt{p/K}$, which shows that two coherent states $|\pm\alpha\rangle_{\text{KPO}_j}$ are the doubly degenerate highest levels of KPO j . We assume that α is sufficiently large so that the

overlap between the coherent states ${}_{\text{KPO}_j} \langle \alpha| - \alpha \rangle_{\text{KPO}_j} = e^{-2\alpha^2}$ is negligible. It is known that these coherent states are stable in the sense that their life time is an exponential function of α^2 [15, Sec. I] [16, Sec. S2]. We use these coherent states to encode logical Kerr-cat qubits:

$$|\bar{0}\rangle_{q_j} := |\alpha\rangle_{\text{KPO}_j}, \quad |\bar{1}\rangle_{q_j} := |-\alpha\rangle_{\text{KPO}_j}. \quad (6)$$

Then, $|\bar{0}, \bar{0}\rangle_q := |\bar{0}\rangle_{q_1} \otimes |\bar{0}\rangle_{q_2}$, $|\bar{0}, \bar{1}\rangle_q$, $|\bar{1}, \bar{0}\rangle_q$, and $|\bar{1}, \bar{1}\rangle_q$ form a complete set of basis states of the two Kerr-cat qubits.

III. SWITCHING OF ZZ COUPLING

Let us explain briefly the mechanism behind the effective ZZ coupling between the Kerr-cat qubits, which is controlled through $\Delta_1(t)$. When $\Delta_1(t) = -\Delta_2$ and $|\Delta_2| \gg g\alpha$, as explained later, four states, $|\bar{i}, \bar{j}\rangle_q \otimes |0, 0\rangle_c$ ($i, j \in \{0, 1\}$), are almost degenerate and the effective coupling between the qubits are suppressed. When $\Delta_1(t) \neq -\Delta_2$, the effective coupling is on. We gradually modulate $\Delta_1(t)$ in order to perform an R_{zz} gate. During the modulation, the states of the Kerr-cat qubits remain $|\bar{i}, \bar{j}\rangle_q$, as verified in the last paragraph of this section; the degeneracy between the two sets of levels corresponding to $\{|\bar{0}, \bar{0}\rangle_q, |\bar{1}, \bar{1}\rangle_q\}$ and $\{|\bar{0}, \bar{1}\rangle_q, |\bar{1}, \bar{0}\rangle_q\}$ is lifted. The energy difference between the two sets of levels can be regarded as the effect of the ZZ-coupling Hamiltonian of the form $E\sigma_z^{q_1}\sigma_z^{q_2}$, where $\sigma_z^{q_j} = (|\bar{0}\rangle_{q_j}\langle\bar{0}| - |\bar{1}\rangle_{q_j}\langle\bar{1}|)/2$ and E is the energy difference.

In order to understand the above mechanism in detail, it is useful to consider the effective Hamiltonians of the couplers conditioned by the state of the Kerr-cat qubits which is assumed to be either of $|\bar{i}, \bar{j}\rangle_q$ ($i, j \in \{0, 1\}$). The effective Hamiltonian corresponding to $|\bar{i}, \bar{j}\rangle_q$ is defined as $\hat{H}_c^{\bar{i}, \bar{j}}(t) = {}_q\langle\bar{i}, \bar{j}|\hat{H}(t)|\bar{i}, \bar{j}\rangle_q$. Using Eq. (6), we obtain

$$\begin{aligned} \hat{H}_c^{\bar{i}, \bar{j}}(t) &= \sum_{k=1}^2 \left[-\frac{\chi}{2} \hat{c}_k^{\dagger 2} \hat{c}_k^2 + \Delta_k(t) \hat{c}_k^{\dagger} \hat{c}_k \right. \\ &\quad \left. + (-1)^i 2g\alpha (\hat{c}_k + \hat{c}_k^{\dagger}) \right] + K\alpha^4 \\ &= \sum_{k=1}^2 \left[-\frac{\chi}{2} \hat{c}_k^{\dagger 2} \hat{c}_k^2 + \Delta_k(t) \left(\hat{c}_k^{\dagger} + \frac{(-1)^i 2g\alpha}{\Delta_k(t)} \right) \right. \\ &\quad \left. \times \left(\hat{c}_k + \frac{(-1)^i 2g\alpha}{\Delta_k(t)} \right) - \frac{4g^2\alpha^2}{\Delta_k(t)} \right] + K\alpha^4 \\ &= \sum_{k=1}^2 \left\{ -\frac{\chi}{2} \hat{c}_k^{\dagger 2} \hat{c}_k^2 + \Delta_k(t) \left[\hat{c}_k^{\dagger} + (-1)^i \alpha_k(t) \right] \right. \\ &\quad \left. \times [\hat{c}_k + (-1)^i \alpha_k(t)] - 2g\alpha\alpha_k(t) \right\} + K\alpha^4, \quad (7) \end{aligned}$$

$$\hat{H}_c^{\bar{i}, \bar{j}(\neq \bar{i})}(t) = \sum_{k=1}^2 \left[-\frac{\chi}{2} \hat{c}_k^{\dagger 2} \hat{c}_k^2 + \Delta_k(t) \hat{c}_k^{\dagger} \hat{c}_k \right] + K\alpha^4, \quad (8)$$

where $\alpha_k(t) = 2g\alpha/\Delta_k(t)$. Note that $\alpha_2 = 2g\alpha/\Delta_2$ is time independent. When the nonlinear terms in Eq. (7) can be neglected, the tensor product of coherent states $|(-1)^{i+1}\alpha_1(t), (-1)^{i+1}\alpha_2\rangle_c$ is the eigenstate of Hamiltonian $H_c^{\bar{i},\bar{i}}(t)$ with eigenenergy

$$E_c^{\bar{i},\bar{i}}(t) := -2g\alpha[\alpha_1(t) + \alpha_2] + K\alpha^4. \quad (9)$$

In this article, we set χ and $|\alpha_k(t)|$ so small that

$${}_{c_k} \left\langle \mp \alpha_k(t) \left| \frac{\chi}{2} \hat{c}_k^\dagger \hat{c}_k^2 \right| \mp \alpha_k(t) \right\rangle_{c_k} = \frac{\chi}{2} \alpha_k(t)^4 \quad (10)$$

can be neglected compared to $2g\alpha\alpha_k(t)$ in Eq. (9); the condition is

$$\chi|\alpha_k(t)|^3 \ll g\alpha. \quad (11)$$

On the other hand, the tensor product of vacuum states $|0, 0\rangle_c$ is the eigenstate of Hamiltonian $H_c^{\bar{i},\bar{j}(\neq\bar{i})}(t)$ with eigenenergy

$$E_c^{\bar{i},\bar{j}(\neq\bar{i})}(t) = K\alpha^4. \quad (12)$$

Suppose that the initial state of the system is represented as

$$|\Psi(0)\rangle = \sum_{i,j=0}^1 \beta_{\bar{i},\bar{j}} |\bar{i},\bar{j}\rangle_q \otimes |0, 0\rangle_c, \quad (13)$$

where $\beta_{\bar{i},\bar{j}}$ is a coefficient. If we set $\Delta_1(0) = -\Delta_2$ and $|\Delta_2| \gg g\alpha$ so that the approximation $|(-1)^{i+1}\alpha_1(0), (-1)^{i+1}\alpha_2\rangle_c \simeq |0, 0\rangle_c$ is valid, $|0, 0\rangle_c$ is not only the eigenstate of $H_c^{\bar{i},\bar{j}(\neq\bar{i})}(0)$ but also the approximate eigenstate of $H_c^{\bar{i},\bar{i}}(0)$. Hence, if we change $\Delta_1(t)$ slowly enough so that coupler 1 evolves adiabatically, the system can evolve as

$$|\Psi(t)\rangle \simeq \sum_{i,j=0}^1 \mathcal{N}(t) \beta_{\bar{i},\bar{j}} e^{-i[\Theta_{\bar{i},\bar{j}}(t) + \theta(t)]} |\bar{i},\bar{j}\rangle_q \otimes |\psi(t)\rangle_c^{\bar{i},\bar{j}}, \quad (14)$$

where

$$\Theta_{\bar{i},\bar{j}}(t) = -\delta_{i,j} \int_0^t 2g\alpha[\alpha_1(t') + \alpha_2] dt'$$

$$= -4g^2\alpha^2 \delta_{i,j} \int_0^t \left[\frac{1}{\Delta_1(t')} + \frac{1}{\Delta_2} \right] dt', \quad (15)$$

$$\theta(t) = K\alpha^4 t, \quad (16)$$

$$|\psi(t)\rangle_c^{\bar{i},\bar{j}} = \delta_{i,j} |(-1)^{i+1}\alpha_1(t), (-1)^{i+1}\alpha_2\rangle_c + (1 - \delta_{i,j}) |0, 0\rangle_c, \quad (17)$$

and $\mathcal{N}(t)$ is for normalization. After the gate time t_f , the detuning of coupler 1 returns to the initial value so that $|\psi(t_f)\rangle_c^{\bar{i},\bar{j}} \simeq |0, 0\rangle_c$. Defining Θ as

$$\Theta = -4g^2\alpha^2 \int_0^{t_f} \left[\frac{1}{\Delta_1(t)} + \frac{1}{\Delta_2} \right] dt, \quad (18)$$

we obtain

$$|\Psi(t_f)\rangle \simeq \sum_{i,j=0}^1 \mathcal{N}(t_f) \beta_{\bar{i},\bar{j}} e^{-i[\Theta\delta_{i,j} + \theta(t_f)]} |\bar{i},\bar{j}\rangle_q \otimes |0, 0\rangle_c \\ = e^{-i\theta(t_f)} R_{zz}(\Theta) |\Psi(0)\rangle =: |\Psi_\Theta^{\text{ideal}}\rangle, \quad (19)$$

where $\theta(t_f)$ is the overall phase which is not of physical interest and

$$R_{zz}(\Theta) := \mathcal{N}(t_f) \sum_{i,j=0}^1 e^{-i\Theta\delta_{i,j}} |\bar{i},\bar{j}\rangle_q \langle \bar{i},\bar{j}| \otimes I_c \quad (20)$$

is the R_{zz} gate with rotation angle Θ on the Kerr-cat qubits with I_c being the identity operator on the couplers. From Eq. (19), we find that the $R_{zz}(\Theta)$ gate is approximately realized. Importantly, we can eliminate an unwanted residual coupling by imposing $\Delta_1(t) = -\Delta_2$, which leads to $\Theta = 0$ in Eq. (18).

In order to verify that the states of the Kerr-cat qubits remain $|\bar{i},\bar{j}\rangle_q$ during the control of $\Delta_1(t)$, we consider the effective drive Hamiltonians of the KPOs conditioned by the state of the couplers, which is either $|(-1)^{i+1}\alpha_1(t), (-1)^{i+1}\alpha_2\rangle_c$ or $|0, 0\rangle_c$. We define the effective drive Hamiltonians corresponding to $|(-1)^{i+1}\alpha_1(t), (-1)^{i+1}\alpha_2\rangle_c$ and $|0, 0\rangle_c$ as

$$\hat{H}_{I,\text{KPO}}^{\bar{i},\bar{i}}(t) := {}_c \left\langle (-1)^{i+1}\alpha_1(t), (-1)^{i+1}\alpha_2 \left| \hat{H}_I \right| (-1)^{i+1}\alpha_1(t), (-1)^{i+1}\alpha_2 \right\rangle_c \\ = (-1)^{i+1} g[\alpha_1(t) + \alpha_2] \sum_{j=1}^2 (\hat{a}_j^\dagger + \hat{a}_j) \quad (21)$$

and

$$\hat{H}_{I,\text{KPO}}^{\bar{i},\bar{j}(\neq\bar{i})} := {}_c \left\langle 0, 0 \left| \hat{H}_I \right| 0, 0 \right\rangle_c = 0, \quad (22)$$

respectively. Since $|\alpha_1(t)|$ and $|\alpha_2|$ are set to be small in

TABLE I. The parameters of the system and detunings. The used values of K and p correspond to $\alpha = 2$. $\kappa/2\pi = 0$ Hz (20 kHz) corresponds to the case without (with) decoherence. These parameters are comparable to those used in experiments [20, 39, 56].

$K/2\pi$	$p/2\pi$	$\chi/2\pi$	$g/2\pi$	$\kappa/2\pi$	α_c^{\min}
20 MHz	80 MHz	10 MHz	10 MHz	0 Hz, 20 kHz	0.04

this study, not only $\hat{H}_{I,\text{KPO}}^{\bar{i},\bar{j}(\neq\bar{i})}$ but also $\hat{H}_{I,\text{KPO}}^{\bar{i},\bar{i}}(t)$ does not deviate the state of the Kerr-cat qubits from $|\bar{i},\bar{j}\rangle_q$ very much.

IV. NUMERICAL RESULTS

We numerically examine the performance of our ZZ -coupling scheme. Time evolution of the system is simulated with the Gorini-Kossakowski-Sudarshan-Lindblad (GKSL)-type Markovian master equation [57, 58]:

$$\begin{aligned} \frac{d\hat{\rho}(t)}{dt} = & -\frac{i}{\hbar}[\hat{H}(t), \hat{\rho}(t)] \\ & + \kappa \sum_{j=1,2} \left(\hat{a}_j \hat{\rho}(t) \hat{a}_j^\dagger - \frac{1}{2} \{ \hat{a}_j^\dagger \hat{a}_j, \hat{\rho}(t) \} \right) \\ & + \kappa \sum_{k=1,2} \left(\hat{c}_k \hat{\rho}(t) \hat{c}_k^\dagger - \frac{1}{2} \{ \hat{c}_k^\dagger \hat{c}_k, \hat{\rho}(t) \} \right), \end{aligned} \quad (23)$$

where $\hat{\rho}(t)$ is the density operator of the system; κ is the single-photon loss rate assumed to be the same for the KPOs and couplers for simplicity; $[\bullet, \circ]$ is the commutator; $\{\bullet, \circ\}$ is the anticommutator. The used system parameters are listed in Table I. The initial state of the system is prepared as in Eq. (13) with $\beta_{\bar{i},\bar{j}} = [2(1+e^{-2\alpha^2})]^{-1}$ $\forall \bar{i}, \bar{j} \in \{0, 1\}$. That is, the four basis states of the Kerr-cat qubits are equally weighted. The initial state can be rewritten as

$$|\Psi(0)\rangle = \frac{|\alpha\rangle_{\text{KPO}_1} + |-\alpha\rangle_{\text{KPO}_1}}{\sqrt{2(1+e^{-2\alpha^2})}} \otimes \frac{|\alpha\rangle_{\text{KPO}_2} + |-\alpha\rangle_{\text{KPO}_2}}{\sqrt{2(1+e^{-2\alpha^2})}} \otimes |0,0\rangle_c, \quad (24)$$

which shows that both of the KPOs are in the even-parity cat states.

In numerical simulations, we used relevant energy eigenstates of isolated KPOs as basis to expand the states of the KPOs instead of their Fock states in order to reduce numerical resource, while Fock states are used for the couplers. In a part of the simulations, we used Quantum Toolbox in Python (QuTiP) [59, 60].

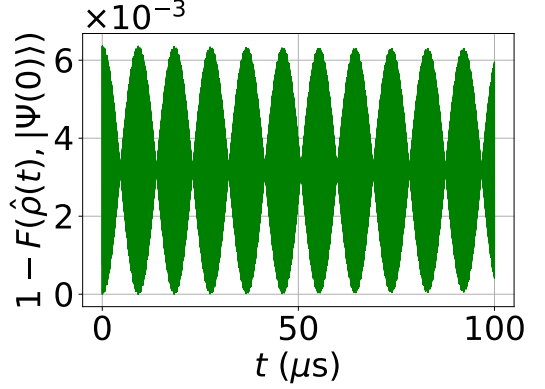


FIG. 2. Infidelity $1 - F(\hat{\rho}(t), |\Psi(0)\rangle)$ when the effective ZZ coupling should be switched off in the case without decoherence. The used parameters are shown in Table I.

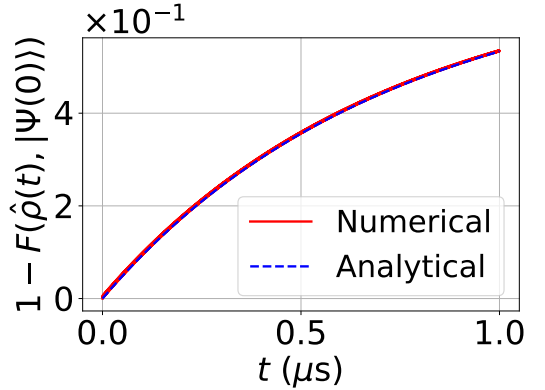


FIG. 3. Infidelity $1 - F(\hat{\rho}(t), |\Psi(0)\rangle)$ when the effective ZZ coupling should be switched off in the case with decoherence. The red solid line labeled “Numerical” is calculated numerically with $\hat{\rho}(t)$ under the master equation (23). The blue dashed line labeled “Analytical” corresponds to Eq. (28). The used parameters are shown in Table I.

A. Residual coupling

We evaluate the performance of our scheme of effective coupling when it is switched off with the infidelity defined as [61, Sec. 9.2.2]

$$1 - F(\hat{\rho}(t), |\Psi(0)\rangle) = 1 - \langle \Psi(0) | \hat{\rho}(t) | \Psi(0) \rangle. \quad (25)$$

We set the detunings of the couplers as follows:

$$\Delta_1(t) = -\Delta_2 = \frac{2g\alpha}{\alpha_c^{\min}} = 2\pi \times 1 \text{ GHz}. \quad (26)$$

Figures 2 and 3 show the infidelity $1 - F(\hat{\rho}(t), |\Psi(0)\rangle)$ for the cases without and with decoherence, respectively. When the decoherence can be neglected, we do not see in Fig. 2 the tendency of the infidelity to increase, which we regard as the sign that the residual coupling is suppressed. We attribute the oscillation in the infidelity to

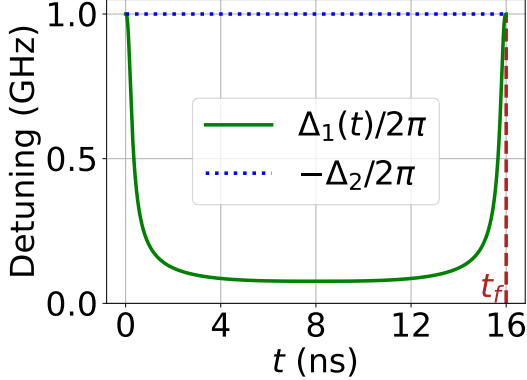


FIG. 4. Time dependence of $\Delta_1(t)$ and $-\Delta_2$ in Eq. (30) for $t_f = 16$ ns and $\alpha_c^{\max} = 0.524$. The other parameters are shown in Table I.

the fact that the initial state is a superposition of different energy eigenstates of the system.

In contrast, when the decoherence cannot be neglected, we see in Fig. 3 the tendency of the infidelity to increase, so we must perform quantum error correction, which is left as our future work. Let us explain this infidelity increase in terms of cat-state dephasing. The dephasing rate due to single-photon loss is given by $\gamma = 2\kappa\alpha^2$ [19, page 6]. If the interaction between the KPOs and the couplers can be neglected, the state of the system at time t is written as [62, Sec. III.B.2]

$$\hat{\rho}(t) = \frac{|\alpha\rangle\langle\alpha| + |-\alpha\rangle\langle-\alpha| + e^{-\gamma t}(|\alpha\rangle\langle-\alpha| + |-\alpha\rangle\langle\alpha|)}{2(1 + e^{-2\alpha^2 - \gamma t})} \otimes \frac{|\alpha\rangle\langle\alpha| + |-\alpha\rangle\langle-\alpha| + e^{-\gamma t}(|\alpha\rangle\langle-\alpha| + |-\alpha\rangle\langle\alpha|)}{2(1 + e^{-2\alpha^2 - \gamma t})} \otimes |0,0\rangle_c\langle 0,0|, \quad (27)$$

where the first (second) line in the right-hand side is the state of KPO 1 (2). Then the infidelity in Eq. (25) is calculated as

$$1 - F(\hat{\rho}(t), |\Psi(0)\rangle) = 1 - \frac{(1 + e^{-2\alpha^2})^2(1 + e^{-\gamma t})^2}{4(1 + e^{-2\alpha^2 - \gamma t})^2}. \quad (28)$$

Since this agrees well with the numerical result as seen from Fig. 3, the neglect of the interaction is validated. In other words, the residual coupling is suppressed in the presence of decoherence, too.

B. Performance of the R_{zz} gate

The R_{zz} gate for the Kerr-cat qubits can be realized by switching on their effective coupling. We evaluate the performance of the R_{zz} gate with the infidelity defined as

$$1 - F(\hat{\rho}(t_f), |\Psi_\Theta^{\text{ideal}}\rangle) = 1 - \langle \Psi_\Theta^{\text{ideal}} | \hat{\rho}(t_f) | \Psi_\Theta^{\text{ideal}} \rangle. \quad (29)$$

We use a particular detuning schedule of the couplers:

$$\Delta_1(t) = \frac{2g\alpha}{\lambda[u(t)]} \quad (0 \leq t \leq t_f), \quad \Delta_2 = -\frac{2g\alpha}{\alpha_c^{\min}}, \quad (30)$$

$$\lambda(x) = \begin{cases} \alpha_c^{\min} + (\alpha_c^{\max} - \alpha_c^{\min}) \left(\frac{x}{T} - \frac{1}{2\pi} \sin \frac{2\pi}{T} x \right) & (0 \leq x \leq T) \\ 2\alpha_c^{\max} - \alpha_c^{\min} - (\alpha_c^{\max} - \alpha_c^{\min}) \\ \times \left(\frac{x}{T} - \frac{1}{2\pi} \sin \frac{2\pi}{T} x \right) & (T \leq x \leq 2T) \end{cases}, \quad (31)$$

where $T = t_f/(\alpha_c^{\max} + \alpha_c^{\min})$ and $u(t)$ is determined from

$$\begin{cases} \alpha_c^{\min}u(t) + (\alpha_c^{\max} - \alpha_c^{\min}) \left\{ \frac{u(t)^2}{2T} - \frac{T}{(2\pi)^2} \right. \\ \times \left. \left[1 - \cos \left(\frac{2\pi}{T}u(t) \right) \right] \right\} = t & (0 \leq t \leq t_f/2) \\ (2\alpha_c^{\max} - \alpha_c^{\min})u(t) - (\alpha_c^{\max} - \alpha_c^{\min}) \left\{ \frac{u(t)^2}{2T} + T \right. \\ \left. - \frac{T}{(2\pi)^2} \left[1 - \cos \left(\frac{2\pi}{T}u(t) \right) \right] \right\} = t & (t_f/2 \leq t \leq t_f) \end{cases}. \quad (32)$$

This corresponds to

$$\alpha_1(t) = \lambda[u(t)], \quad \alpha_2 = -\alpha_c^{\min}. \quad (33)$$

Note that we have

$$\lambda(2T - x) = \lambda(x) \quad (0 \leq x \leq T), \quad (34)$$

$$u(0) = 0, \quad u(t_f/2) = T, \quad u(t_f) = 2T, \quad (35)$$

$$\lambda[u(0)] = \lambda[u(t_f)] = \alpha_c^{\min}, \quad \lambda[u(t_f/2)] = \alpha_c^{\max}, \quad (36)$$

$$\Delta_1(0) = \Delta_1(t_f) = -\Delta_2 = 2g\alpha/\alpha_c^{\min} = 2\pi \times 1 \text{ GHz}. \quad (37)$$

The complicated form of $\lambda[u(t)]$ is the result of trial and error. Predetermined parameters are listed in Table I. In calculations of the infidelity for each gate time t_f , we optimize α_c^{\max} so that we have the minimal infidelity with $\Theta = -\pi/2$. We fix $\Theta = -\pi/2$ because R_{zz} and R_x (X -rotation) gates with rotation angle $-\pi/2$ and the R_z (Z -rotation) gate with all rotation angles are sufficient to form a universal gate set [18]. The used values of α_c^{\max} are listed in Table II. Typical time dependence of $\Delta_1(t)$ is presented in Fig. 4. The point is that we decrease $\Delta_1(t)$ as rapidly as possible while avoiding nonadiabatic transitions after $t = 0$ and keep it at a small value most of the gate time while keeping α_c^{\max} not too large. This is because we must satisfy the condition (11).

Figure 5 shows the infidelity $1 - F(\hat{\rho}(t_f), |\Psi_\Theta^{\text{ideal}}\rangle)$ as a function of t_f in the cases with and without decoherence. First, let us focus on the case without decoherence. We find that the gate fidelity is over 99.9% for $t_f = 16$ ns. When $t_f \lesssim 16$ ns, the gate infidelity tends to decrease

TABLE II. α_c^{\max} that minimizes the infidelity $1 - F(\hat{\rho}(t_f), |\Psi_\Theta^{\text{ideal}}\rangle)$ for each gate time t_f .

t_f (ns)	8	10	12	14	15	16	17	18	19	20	21	22	24	26	28	30
α_c^{\max}	0.404	0.460	0.496	0.524	0.528	0.524	0.510	0.486	0.468	0.440	0.412	0.408	0.390	0.370	0.336	0.314
t_f (ns)	32	34	36	38	40	42	44	46	48	50	52	54	56	58	60	
α_c^{\max}	0.318	0.296	0.280	0.264	0.252	0.244	0.232	0.226	0.230	0.212	0.220	0.202	0.198	0.192	0.188	

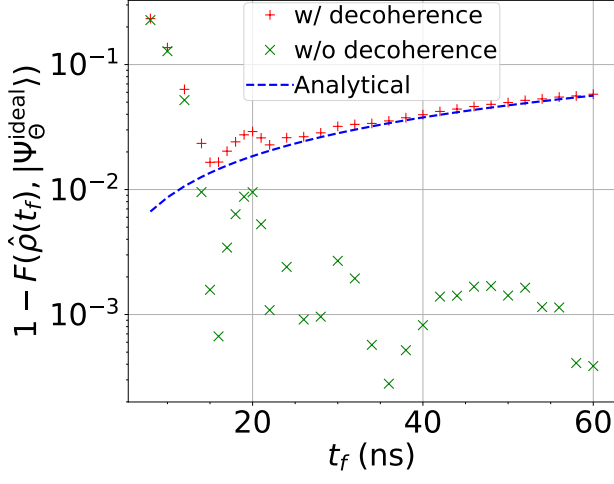


FIG. 5. Infidelity of the $R_{zz}(-\pi/2)$ gate as a function of t_f , with and without decoherence. The blue dashed line labeled “Analytical” corresponds to Eq. (40). The used parameters and α_c^{\max} are listed in Table I and Table II, respectively.

with the increase of t_f due to the mitigation of nonadiabatic transitions. On the other hand, when $t_f \gtrsim 16$ ns, the tendency is not seen in spite of further suppression of nonadiabatic transitions. The infidelity is not lower than 10^{-4} in the range of t_f studied. We attribute these to the fact that $|\bar{i}, \bar{j}\rangle_q \otimes |\psi(t)\rangle_c^{\bar{i}, \bar{j}}$ in Eq. (14) is not an exact eigenstate of the total Hamiltonian.

Next, let us focus on the effect of decoherence. When $t_f \lesssim 12$ ns, the effect is small, and the infidelities with and without decoherence are almost the same. Otherwise, decoherence makes the infidelity larger; when $t_f \gtrsim 22$ ns, the infidelity monotonically increases with t_f . Let us explain this monotonic increase in a similar way with that in the last paragraph in the previous subsection. From Eq. (19), we have

$$|\Psi_\Theta^{\text{ideal}}\rangle \langle \Psi_\Theta^{\text{ideal}}| = \sum_{i,i',j,j'=0}^1 \frac{e^{i\Theta(\delta_{i',j'} - \delta_{i,j})}}{4(1 + 2 \cos \Theta e^{-2\alpha^2} + e^{-4\alpha^2})} \times |\bar{i}\rangle_{q_1} \langle \bar{i}| \otimes |\bar{j}\rangle_{q_2} \langle \bar{j}| \otimes |0,0\rangle_c \langle 0,0|. \quad (38)$$

This state does not include the effect of dephasing. The counterpart with the effect is given by

$$\hat{\rho}_\Theta^{\text{dephased}}(t_f)$$

$$= \sum_{i,i',j,j'=0}^1 \frac{e^{i\Theta(\delta_{i',j'} - \delta_{i,j}) - \gamma t_f(2 - \delta_{i,i'} - \delta_{j,j'})}}{4(1 + 2 \cos \Theta e^{-2\alpha^2} - \gamma t_f + e^{-4\alpha^2 - 2\gamma t_f})} \times |\bar{i}\rangle_{q_1} \langle \bar{i}| \otimes |\bar{j}\rangle_{q_2} \langle \bar{j}| \otimes |0,0\rangle_c \langle 0,0|. \quad (39)$$

The infidelity only due to the effect of dephasing is calculated as

$$\begin{aligned} & 1 - F(\hat{\rho}_\Theta^{\text{dephased}}(t_f), |\Psi_\Theta^{\text{ideal}}\rangle) \\ &= 1 - 4^{-1} [(1 + e^{-\gamma t_f})^2 (1 + e^{-4\alpha^2}) \\ &\quad \times (1 + 4 \cos \Theta e^{-2\alpha^2} + e^{-4\alpha^2}) \\ &\quad + 4e^{-4\alpha^2} (1 + 2 \cos 2\Theta e^{-\gamma t_f} + e^{-2\gamma t_f})] \\ &\quad \times (1 + 2 \cos \Theta e^{-2\alpha^2} + e^{-4\alpha^2})^{-1} \\ &\quad \times (1 + 2 \cos \Theta e^{-2\alpha^2 - \gamma t_f} + e^{-4\alpha^2 - 2\gamma t_f})^{-1}. \end{aligned} \quad (40)$$

As this agrees well with the numerical result in Fig. 5, the infidelity increase for large t_f is mostly due to dephasing.

V. CONCLUSION

We have developed a tunable ZZ -coupling scheme between two Kerr-cat qubits by using two transmon couplers. The detuning of one of the couplers is tuned to control the coupling amplitude. We have analytically presented and numerically confirmed that the residual coupling is eliminated by setting the detunings of the transmon couplers to values opposite to each other. We have numerically achieved $R_{zz}(-\pi/2)$ -gate fidelity over 99.9% in the case of 16-ns gate time and without decoherence.

As we have seen in Figs. 3 and 5, the effect of decoherence is serious. In order to preserve superposition states of Kerr-cat qubits, we must perform quantum error correction. Combining our ZZ -coupling scheme with quantum error correction is left for future works.

ACKNOWLEDGMENTS

The authors thank Yuichiro Matsuzaki, Toyofumi Ishikawa, and Hiroomi Chono for useful discussion. This paper is based on results obtained from a project, JPNP16007, commissioned by the New Energy and Industrial Technology Development Organization (NEDO), Japan.

[1] M. A. Nielsen and I. L. Chuang, *Quantum Computation and Quantum Information: 10th Anniversary Edition* (Cambridge University Press, 2010).

[2] P. W. Shor, Polynomial-Time Algorithms for Prime Factorization and Discrete Logarithms on a Quantum Computer, *SIAM Review* **41**, 303 (1999).

[3] L. K. Grover, A fast quantum mechanical algorithm for database search, in *Proceedings of the Twenty-Eighth Annual ACM Symposium on Theory of Computing*, STOC '96 (Association for Computing Machinery, New York, NY, USA, 1996) p. 212–219.

[4] S. McArdle, S. Endo, A. Aspuru-Guzik, S. C. Benjamin, and X. Yuan, Quantum computational chemistry, *Rev. Mod. Phys.* **92**, 015003 (2020).

[5] J. Biamonte, P. Wittek, N. Pancotti, P. Rebentrost, N. Wiebe, and S. Lloyd, Quantum machine learning, *Nature* **549**, 195 (2017).

[6] M. A. Schlosshauer, *Decoherence and the Quantum-To-Classical Transition* (Springer, Berlin, Heidelberg, 2007).

[7] M. Schlosshauer, Quantum decoherence, *Physics Reports* **831**, 1 (2019).

[8] S. J. Devitt, W. J. Munro, and K. Nemoto, Quantum error correction for beginners, *Reports on Progress in Physics* **76**, 076001 (2013).

[9] J. Roffe, Quantum error correction: an introductory guide, *Contemporary Physics* **60**, 226 (2019).

[10] J. Preskill, Quantum Computing in the NISQ era and beyond, *Quantum* **2**, 79 (2018).

[11] P. Webster, S. D. Bartlett, and D. Poulin, Reducing the overhead for quantum computation when noise is biased, *Phys. Rev. A* **92**, 062309 (2015).

[12] S. Puri, L. St-Jean, J. A. Gross, A. Grimm, N. E. Frattini, P. S. Iyer, A. Krishna, S. Touzard, L. Jiang, A. Blais, S. T. Flammia, and S. M. Girvin, Bias-preserving gates with stabilized cat qubits, *Science Advances* **6**, eaay5901 (2020).

[13] Y.-H. Chen, R. Stassi, W. Qin, A. Miranowicz, and F. Nori, Fault-Tolerant Multiqubit Geometric Entangling Gates Using Photonic Cat-State Qubits, *Phys. Rev. Appl.* **18**, 024076 (2022).

[14] Q. Xu, J. K. Iverson, F. G. S. L. Brandão, and L. Jiang, Engineering fast bias-preserving gates on stabilized cat qubits, *Phys. Rev. Research* **4**, 013082 (2022).

[15] S. Puri, A. Grimm, P. Campagne-Ibarcq, A. Eickbusch, K. Noh, G. Roberts, L. Jiang, M. Mirrahimi, M. H. Devoret, and S. M. Girvin, Stabilized Cat in a Driven Nonlinear Cavity: A Fault-Tolerant Error Syndrome Detector, *Phys. Rev. X* **9**, 041009 (2019).

[16] Y. Suzuki, S. Watabe, S. Kawabata, and S. Masuda, Measurement-based preparation of stable coherent states of a Kerr parametric oscillator, *Scientific Reports* **13**, 1606 (2023).

[17] P. T. Cochrane, G. J. Milburn, and W. J. Munro, Macroscopically distinct quantum-superposition states as a bosonic code for amplitude damping, *Phys. Rev. A* **59**, 2631 (1999).

[18] H. Goto, Universal quantum computation with a nonlinear oscillator network, *Phys. Rev. A* **93**, 050301(R) (2016).

[19] S. Puri, S. Boutin, and A. Blais, Engineering the quantum states of light in a Kerr-nonlinear resonator by two-photon driving, *npj Quantum Information* **3**, 18 (2017).

[20] A. Grimm, N. E. Frattini, S. Puri, S. O. Mundhada, S. Touzard, M. Mirrahimi, S. M. Girvin, S. Shankar, and M. H. Devoret, Stabilization and operation of a Kerr-cat qubit, *Nature* **584**, 205 (2020).

[21] H. Goto, Bifurcation-based adiabatic quantum computation with a nonlinear oscillator network, *Scientific Reports* **6**, 21686 (2016).

[22] S. E. Nigg, N. Lörch, and R. P. Tiwari, Robust quantum optimizer with full connectivity, *Science Advances* **3**, e1602273 (2017).

[23] S. Puri, C. K. Andersen, A. L. Grimsmo, and A. Blais, Quantum annealing with all-to-all connected nonlinear oscillators, *Nature Communications* **8**, 15785 (2017).

[24] P. Zhao, Z. Jin, P. Xu, X. Tan, H. Yu, and Y. Yu, Two-Photon Driven Kerr Resonator for Quantum Annealing with Three-Dimensional Circuit QED, *Phys. Rev. Applied* **10**, 024019 (2018).

[25] H. Goto, Quantum Computation Based on Quantum Adiabatic Bifurcations of Kerr-Nonlinear Parametric Oscillators, *Journal of the Physical Society of Japan* **88**, 061015 (2019).

[26] M. J. Kewming, S. Shrapnel, and G. J. Milburn, Quantum correlations in the Kerr Ising model, *New Journal of Physics* **22**, 053042 (2020).

[27] T. Onodera, E. Ng, and P. L. McMahon, A quantum annealer with fully programmable all-to-all coupling via Floquet engineering, *npj Quantum Information* **6**, 48 (2020).

[28] H. Goto and T. Kanao, Quantum annealing using vacuum states as effective excited states of driven systems, *Communications Physics* **3**, 235 (2020).

[29] T. Kanao and H. Goto, High-accuracy Ising machine using Kerr-nonlinear parametric oscillators with local four-body interactions, *npj Quantum Information* **7**, 18 (2021).

[30] T. Yamaji, M. Shirane, and T. Yamamoto, Development of Quantum Annealer Using Josephson Parametric Oscillators, *IEICE Transactions on Electronics* **E105.C**, 283 (2022).

[31] H. Goto, Z. Lin, and Y. Nakamura, Boltzmann sampling from the Ising model using quantum heating of coupled nonlinear oscillators, *Scientific Reports* **8**, 7154 (2018).

[32] S. Masuda, T. Ishikawa, Y. Matsuzaki, and S. Kawabata, Controls of a superconducting quantum parametron under a strong pump field, *Scientific Reports* **11**, 11459 (2021).

[33] A. S. Darmawan, B. J. Brown, A. L. Grimsmo, D. K. Tuckett, and S. Puri, Practical Quantum Error Correction with the XZZX Code and Kerr-Cat Qubits, *PRX Quantum* **2**, 030345 (2021).

[34] H. Putterman, J. Iverson, Q. Xu, L. Jiang, O. Painter, F. G. S. L. Brandão, and K. Noh, Stabilizing a Bosonic Qubit Using Colored Dissipation, *Phys. Rev. Lett.* **128**, 110502 (2022).

[35] Y.-H. Kang, Y.-H. Chen, X. Wang, J. Song, Y. Xia, A. Miranowicz, S.-B. Zheng, and F. Nori, Nonadiabatic geometric quantum computation with cat-state qubits via invariant-based reverse engineering, *Phys. Rev. Res.* **4**, 013233 (2022).

[36] T. Kanao, S. Masuda, S. Kawabata, and H. Goto, Quan-

tum Gate for a Kerr Nonlinear Parametric Oscillator Using Effective Excited States, *Phys. Rev. Appl.* **18**, 014019 (2022).

[37] S. Masuda, T. Kanao, H. Goto, Y. Matsuzaki, T. Ishikawa, and S. Kawabata, Fast Tunable Coupling Scheme of Kerr Parametric Oscillators Based on Shortcuts to Adiabaticity, *Phys. Rev. Appl.* **18**, 034076 (2022).

[38] H. Chono, T. Kanao, and H. Goto, Two-qubit gate using conditional driving for highly detuned Kerr nonlinear parametric oscillators, *Phys. Rev. Res.* **4**, 043054 (2022).

[39] T. Yamaji, S. Kagami, A. Yamaguchi, T. Satoh, K. Koshino, H. Goto, Z. R. Lin, Y. Nakamura, and T. Yamamoto, Spectroscopic observation of the crossover from a classical Duffing oscillator to a Kerr parametric oscillator, *Phys. Rev. A* **105**, 023519 (2022).

[40] T. Yamaji, S. Masuda, A. Yamaguchi, T. Satoh, A. Morioka, Y. Igarashi, M. Shirane, and T. Yamamoto, Correlated oscillations in Kerr parametric oscillators with tunable effective coupling, *arXiv e-prints*, [arXiv:2212.13682](https://arxiv.org/abs/2212.13682) (2022).

[41] M. Sarovar, T. Proctor, K. Rudinger, K. Young, E. Nielsen, and R. Blume-Kohout, Detecting crosstalk errors in quantum information processors, *Quantum* **4**, 321 (2020).

[42] Y. Ding, P. Gokhale, S. Lin, R. Rines, T. Propson, and F. T. Chong, Systematic Crosstalk Mitigation for Superconducting Qubits via Frequency-Aware Compilation, in *2020 53rd Annual IEEE/ACM International Symposium on Microarchitecture (MICRO)* (IEEE Computer Society, Los Alamitos, CA, USA, 2020) pp. 201–214.

[43] Y. Chen, C. Neill, P. Roushan, N. Leung, M. Fang, R. Barends, J. Kelly, B. Campbell, Z. Chen, B. Chiaro, A. Dunsworth, E. Jeffrey, A. Megrant, J. Y. Mutus, P. J. J. O’Malley, C. M. Quintana, D. Sank, A. Vainsencher, J. Wenner, T. C. White, M. R. Geller, A. N. Cleland, and J. M. Martinis, Qubit Architecture with High Coherence and Fast Tunable Coupling, *Phys. Rev. Lett.* **113**, 220502 (2014).

[44] F. Yan, P. Krantz, Y. Sung, M. Kjaergaard, D. L. Campbell, T. P. Orlando, S. Gustavsson, and W. D. Oliver, Tunable Coupling Scheme for Implementing High-Fidelity Two-Qubit Gates, *Phys. Rev. Applied* **10**, 054062 (2018).

[45] P. Mundada, G. Zhang, T. Hazard, and A. Houck, Suppression of Qubit Crosstalk in a Tunable Coupling Superconducting Circuit, *Phys. Rev. Applied* **12**, 054023 (2019).

[46] X. Li, T. Cai, H. Yan, Z. Wang, X. Pan, Y. Ma, W. Cai, J. Han, Z. Hua, X. Han, Y. Wu, H. Zhang, H. Wang, Y. Song, L. Duan, and L. Sun, Tunable Coupler for Realizing a Controlled-Phase Gate with Dynamically Decoupled Regime in a Superconducting Circuit, *Phys. Rev. Applied* **14**, 024070 (2020).

[47] P. Zhao, P. Xu, D. Lan, J. Chu, X. Tan, H. Yu, and Y. Yu, High-Contrast ZZ Interaction Using Superconducting Qubits with Opposite-Sign Anharmonicity, *Phys. Rev. Lett.* **125**, 200503 (2020).

[48] J. Ku, X. Xu, M. Brink, D. C. McKay, J. B. Hertzberg, M. H. Ansari, and B. L. T. Plourde, Suppression of Unwanted ZZ Interactions in a Hybrid Two-Qubit System, *Phys. Rev. Lett.* **125**, 200504 (2020).

[49] J. Stehlik, D. M. Zajac, D. L. Underwood, T. Phung, J. Blair, S. Carnevale, D. Klaus, G. A. Keefe, A. Carniol, M. Kumph, M. Steffen, and O. E. Dial, Tunable Coupling Architecture for Fixed-Frequency Transmon Superconducting Qubits, *Phys. Rev. Lett.* **127**, 080505 (2021).

[50] C. Leroux, A. Di Paolo, and A. Blais, Superconducting Coupler with Exponentially Large On:Off Ratio, *Phys. Rev. Appl.* **16**, 064062 (2021).

[51] H. Goto, Double-Transmon Coupler: Fast Two-Qubit Gate with No Residual Coupling for Highly Detuned Superconducting Qubits, *Phys. Rev. Appl.* **18**, 034038 (2022).

[52] G. S. Paraoanu, Microwave-induced coupling of superconducting qubits, *Phys. Rev. B* **74**, 140504(R) (2006).

[53] C. Rigetti and M. Devoret, Fully microwave-tunable universal gates in superconducting qubits with linear couplings and fixed transition frequencies, *Phys. Rev. B* **81**, 134507 (2010).

[54] S. Sheldon, E. Magesan, J. M. Chow, and J. M. Gambetta, Procedure for systematically tuning up cross-talk in the cross-resonance gate, *Phys. Rev. A* **93**, 060302(R) (2016).

[55] M. Malekakhlagh, E. Magesan, and D. C. McKay, First-principles analysis of cross-resonance gate operation, *Phys. Rev. A* **102**, 042605 (2020).

[56] Z. Wang, M. Pechal, E. A. Wollack, P. Arrangoiz-Arriola, M. Gao, N. R. Lee, and A. H. Safavi-Naeini, Quantum Dynamics of a Few-Photon Parametric Oscillator, *Phys. Rev. X* **9**, 021049 (2019).

[57] V. Gorini, A. Kossakowski, and E. C. G. Sudarshan, Completely positive dynamical semigroups of N -level systems, *Journal of Mathematical Physics* **17**, 821 (1976).

[58] G. Lindblad, On the generators of quantum dynamical semigroups, *Communications in Mathematical Physics* **48**, 119 (1976).

[59] J. Johansson, P. Nation, and F. Nori, QuTiP: An open-source Python framework for the dynamics of open quantum systems, *Computer Physics Communications* **183**, 1760 (2012).

[60] J. Johansson, P. Nation, and F. Nori, QuTiP 2: A Python framework for the dynamics of open quantum systems, *Computer Physics Communications* **184**, 1234 (2013).

[61] M. M. Wilde, *Quantum Information Theory*, 2nd ed. (Cambridge University Press, 2017).

[62] P. Krantz, M. Kjaergaard, F. Yan, T. P. Orlando, S. Gustavsson, and W. D. Oliver, A quantum engineer’s guide to superconducting qubits, *Applied Physics Reviews* **6**, 021318 (2019).